HHS Public Access

Author manuscript

Nat Cell Biol. Author manuscript; available in PMC 2012 July 24.

Published in final edited form as:

Nat Cell Biol. 2011 January ; 13(1): 40–48. doi:10.1038/ncb2132.

Myosin-Va Transports the Endoplasmic Reticulum into the Dendritic Spines of Purkinje Neurons

Wolfgang Wagner[1], **Stephan D. Brenowitz**[2], and **John A. Hammer III**[1]

[1]Laboratory of Cell Biology, National Heart, Lung, and Blood Institute, National Institutes of Health, Bethesda, MD 20892, USA

[2]Section on Synaptic Transmission, National Institute on Deafness and Other Communication Disorders, National Institutes of Health, Bethesda, MD 20892, USA

Abstract

Extension of the endoplasmic reticulum (ER) into dendritic spines of Purkinje neurons (PNs) is required for cerebellar synaptic plasticity and is disrupted in animals with null mutations in *Myo5a*, the gene encoding myosin-Va[1–3]. Notably, the mechanism ensuring the ER's localization to spines has not been unraveled. While it has been proposed that animal class V myosins localize organelles by tethering them to the actin cytoskeleton[4–7], we demonstrate here that myosin-Va acts as a point-to-point organelle transporter to pull ER as cargo into PN spines. Specifically, the myosin accumulates at the ER tip as the organelle moves into spines, and the myosin's ability to hydrolyze ATP is required for spine ER targeting. Moreover, myosin-Va is responsible for the vast majority of spine ER insertional events. Finally, attenuation of the myosin's ability to move along actin filaments reduces the maximum velocity of ER movement into spines, providing direct evidence that myosin-Va drives ER motility. Thus, we establish that an actin-based motor moves ER within animal cells, and we uncover the mechanism that mediates ER localization to PN spines, a prerequisite for synaptic plasticity.

Class V myosins are actin-based motors that mediate the proper intracellular localization of diverse organelles, mRNAs and proteins[3]. There is convincing evidence that myosin-V drives the motility of organelles along actin filaments in *Saccharomyces*[8] and *Dictyostelium*[9]. In metazoans, however, a role for class V myosins as point-to-point cargo transporters has been questioned despite the fact that these myosins possess features that are ideal for driving organelle transport[3]. Rather, it has been suggested that they function primarily by tethering organelles to the actin cytoskeleton[4, 6, 7] or to the plasma membrane[5] after delivery by microtubule-based transport.

The heavy chain of mouse myosin-Va is encoded by *Dilute* (*Myo5a*), one of three class V myosin genes present in mammals[3]. Myosin-Va is recruited to melanosomes to mediate their accumulation in the actin-rich periphery of melanocytes[3, 7]. Therefore, *dilute* mutations

Author Contributions W.W. and J.A.H. designed the project. W.W. carried out the experiments except the Ca^{2+} imaging, which was carried out by S.D.B.. J.A.H. contributed new reagents and W.W., S.D.B. and J.A.H. analyzed the data and wrote the manuscript.

cause pigmentation defects. In addition, mice homozygous for *dilute-lethal* alleles such as d^{l20J}, a functional null allele of *Myo5a*, display severe ataxia[10]. This phenotype, together with the high level of *Myo5a* expression in cerebellar PNs[11], suggest a role for myosin-Va in the cerebellum. Consistently, *dilute-lethal* PNs *in situ* display a striking organelle localization defect, as ER is missing specifically from their dendritic spines[1, 2].

Dendritic spines are small, actin-rich protrusions on neuronal dendrites that serve as sites of excitatory synaptic input and constitute postsynaptic signaling micro-compartments[12]. The ER, a dynamic organelle consisting of a continuous network of membrane tubules and cisternae[13], normally extends into all PN spines[12]. This spine ER releases Ca^{2+} locally via the type 1 inositol 1,4,5-trisphosphate receptor (Itpr1) in response to IP3 produced after metabotropic glutamate receptor (mGluR) activation, thereby facilitating mGluR-dependent long-term depression (LTD)[1, 14–16], a form of synaptic plasticity thought to underlie cerebellar motor learning[14, 17]. Importantly, the mGluR-dependent Ca^{2+} transient evoked in PN spines by parallel fiber (PF) stimulation is attenuated by ~50% in *dilute-lethal* PNs and LTD at the PF-PN synapse is abolished in this mutant[1].

To confirm that the myosin-Va-dependent localization of ER to spines is essential for the local Ca^{2+} signal elicited by mGluR-activation, we used two-photon laser glutamate uncaging to stimulate individual PN spines in acute cerebellar slices. PNs were loaded with the Ca^{2+} indicator Fluo-4 and Alexa-594 to visualize cell volume (Fig. 1a, upper panel). Glutamate was uncaged at single spine heads (Fig. 1a, lower panel) in the presence of the AMPA-receptor inhibitor DNQX, producing a long-latency Ca^{2+} transient (167 ± 12 msec, range 80 to 330 msec) in the spine but not in the dendritic shaft of control PNs (Fig. 1b; d^{v}/d^{l20J} + DNQX; *left*: traces from a single spine/dendrite pair; *middle*: average trace; see Methods for explanation of genotypes). This spine Ca^{2+} transient requires mGluR1 activation (Fig. 1b; d^{v}/d^{l20J} + DNQX/CPCCOEt) and is entirely absent in the spines of d^{l20J}/d^{l20J} PNs (Fig. 1c; d^{l20J}/d^{l20J} + DNQX; see Fig.1d for a comparison of peak Ca^{2+} magnitudes). Notably, AMPA-receptor-dependent, fast Ca^{2+} transients in spines following glutamate uncaging are preserved in d^{l20J}/d^{l20J} PNs (Supplementary Information, Fig. S1). These results verify that the mGluR-dependent Ca^{2+} transient evoked locally within PN spines depends on myosin-Va and the presence of spine ER.

Given the physiological importance of localizing ER to spines, we next asked how myosin-Va is involved in targeting the ER to these protrusions. There are at least three likely mechanisms for how the myosin might function in this process. First, myosin-Va might function in a non-cell autonomous manner, e.g. in the presynaptic neuron, to confer upon PNs the ability to localize ER to spines (Mechanism 1; Fig. 1e). Second, myosin-Va might function within the PN to mediate the tethering of ER in spines after the organelle has been transported into the spine by a myosin-Va-independent mechanism (Mechanism 2; Fig. 1f). Third, myosin-Va might function as a cargo transporter that associates with ER and moves it along actin filaments into spines (Mechanism 3; Fig. 1g).

To investigate the role of myosin-Va in ER localization, we initially analyzed the dynamic behavior of this organelle in PN spines in dissociated cerebellar cultures from wild type (WT) mice (Fig. 2a–d). For this and all subsequent experiments, the cerebellar cultures were

transfected by nucleofection with novel plasmids harboring a PN-specific promotor[18] that drives expression of inserted cDNAs specifically in the PNs present within these heterogenous cultures (W.W., Seumas McCroskery, and J.A.H., manuscript in preparation; see also Methods). To visualize the PN's ER and cell volume, we used a plasmid encoding both an mRFP-tagged protein that targets to the ER lumen (mRFPER)[19] and a cell volume marker (GFP). Consistent with previous observations of fixed cerebellar sections[1, 20], confocal microscopy of live PNs at day *in vitro* (DIV) 15 shows that almost all spines are fully loaded ER (Fig. 2a; Fig. 5a). Notably, the ER is continuously present within these spines during the time of observation (Fig. 2b; Supplementary Movies 1, 2). In contrast, analysis of the steady state presence of spine ER at 10 DIV (when PN dendrites are starting to grow out; Fig. 2c) shows that ∼13% of spine-like protrusions are either empty or only partially filled with ER at any given moment (Supplementary Information, Fig. S2a). Strikingly, events where ER translocates into these protrusions by progressively extending towards the protrusion's tip are common (Fig. 2d; Supplementary Information, Fig. S2b, Movies 1, 2). Retractions of spine ER are also observed at this stage (Supplementary Fig. S2c). Therefore, both ER translocation and ER maintenance potentially contribute to the localization of ER to spines.

To discriminate whether the loss of myosin-Va affects the translocation of ER into spines, or simply the maintenance/tethering of ER within these protrusions, we observed the ER in live d^{l20J}/d^{l20J} PNs (Fig. 2e–h). If only the ER's maintenance within spines is myosin-Va-dependent, then the organelle would be expected to move at least transiently into d^{l20J}/d^{l20J} spines in search of myosin-Va-dependent tethering. Consistent with previous analyses of mutant PNs *in situ*[1, 2], the ER is still present within the dendrites of d^{l20J}/d^{l20J} PNs, but it is almost completely missing from their spines at 15 DIV (Fig. 2e; Fig. 5a) and at 10 DIV (Fig. 2g; Supplementary Information, Fig. S2a). Importantly, time-lapse recording of live 10 DIV cultures shows that the frequency of ER movement into empty/partially-filled spines is reduced ∼30-fold in d^{l20J}/d^{l20J} PNs relative to control PNs (Fig. 2h; Supplementary Information, Fig. S2b, Movies 3, 4). Therefore, the movement of ER into PN spines depends critically on myosin-Va. This effectively rules out Mechanism 2 (Fig. 1f), which requires that the movement of ER into spines be driven by a myosin-Va-independent mechanism.

While the ER insertional frequency data argues that the vast majority of these events are driven by myosin-Va, rare myosin-Va-independent insertional events do occur (Supplementary Information, Fig. S2b) and could contribute over time to spine ER targeting. Since microtubules mediate ER motility in animal cells[13] and transiently grow into dendritic spines of hippocampal neurons[21] and PNs (Supplementary Information, Fig. S3a), we asked whether microtubules contribute to the movement of ER into PN spines. Importantly, while low-dose nocodazole blocks microtubule entry into PN spines, it does not reduce the frequency of ER movement into spines of control d^{v}/d^{l20J} PNs (Supplementary Information, Fig. S3a,e). Moreover, the frequency of microtubule growth into spines is not diminished in d^{l20J}/d^{l20J} PNs (Supplementary Information, Fig. S3b), indicating that the dramatic loss of ER insertional movement seen in the absence of myosin-Va is not caused by failure of microtubules to enter spines. Interestingly, the rare ER insertional events seen in d^{l20J}/d^{l20J} PNs (Supplementary Information, Fig. S2b) are always accompanied by microtubule entry

and are abolished by low-dose nocodazole treatment (Supplementary Information, Fig. S3c,e). Taken together, these results show that while microtubule-dependent ER insertion into PN spines can occur, its contribution to the transport of ER into spines in WT PNs must be very minor.

Consistent with previous electron microscopy studies[2, 20], control experiments (Supplementary Information, Fig. S4, S5, Movie 5) argue that the ER targeting defect in d^{l20J}/d^{l20J} PNs is not due to a general disruption of spine organization or the targeting of postsynaptic density (PSD) proteins, although the morphology of the dendritic arbor is affected somewhat in cultured d^{l20J}/d^{l20J} PNs at 15 DIV and later (Supplementary Information, Fig. S6). Since cultured PNs receive presynaptic input from granule neurons both *in vivo*[14] and in culture[22], and PN development is affected by brain-derived neurotrophic factor secreted by granule neurons[23], we considered the possibility that myosin-Va triggers the targeting of ER to PN spines by functioning non-cell autonomously (Mechanism 1; Fig. 1e). To determine if the presence of myosin-Va within PNs is sufficient for localizing the ER to PN spines, cerebellar cultures from d^{l20J}/d^{l20J} mice were transfected with PN-specific plasmids expressing a GFP-tagged version of the brain-spliced isoform of myosin-Va and mRFP-ER. Strikingly, this restores the characteristic tubular ER that protrudes from the dendritic shaft into spines in the d^{l20J}/d^{l20J} PNs (Fig. 3a, b, and top panels in d). Moreover, mGFP-myosin-Va localizes to the tip of the spine ER (see the maximum projection image of a Z-stack in Fig. 3a, the corresponding three-dimensional reconstruction in Supplementary Movie 6, and the examples of single confocal plane images in Fig. 3b), and it remains concentrated there over time, even as these ER tubules grow and shrink, as evidenced by kymograph images (Fig. 3c; see also Supplementary Movies 7–9). To quantify the extent to which ER targeting is rescued, and to confirm that the ER is continuously present in rescued spines as in WT spines at 15 DIV, we expressed a volume marker (GFP) in addition to mRFP-ER and mGFP-myosin-Va in d^{l20J}/d^{l20J} PNs. Analysis of these PNs showed that ER targeting is rescued to the level of WT PNs (Fig. 5a). In addition, time-lapse imaging reveals that the ER is continuously maintained in these spines (Supplementary Movie 10, top panels). Since the exogenous, GFP-tagged myosin-Va is expressed specifically within the PNs present in these mixed cultures (Fig. 3d, top panel), myosin-Va must function within PNs to mediate ER targeting. Consistent with this, ER targeting is not rescued in d^{l20J}/d^{l20J} PNs when co-cultured with cerebellar cells from WT mice (Supplementary Information, Fig. S7). Therefore, despite the fact that myosin-Va could have important functions in other cerebellar cell types, these results argue strongly against Mechanism 1.

To determine whether the myosin's motor activity is necessary for ER targeting, we transfected d^{l20J}/d^{l20J} PNs with plasmids encoding myosin-Va with mutations known (G440A and E442A)[24] or expected (R219A)[25] to severely impair its steady state ATPase activity. None of the mutant versions of myosin-Va was able to rescue ER targeting (Fig. 3d; Supplementary Movie 9). Thus, ER translocation is dependent on the myosin's ability to hydrolyze ATP. Because the G440A mutation traps myosin-Va in a state with relatively high affinity for actin at physiological ATP levels[24], these data also suggest that the myosin's ability to simply link its cargo to F-actin is not sufficient for ER targeting.

If myosin-Va pulls ER as cargo into spines, then the myosin is expected to associate with the spine ER. Several observations indicate that this is the case. First, the striking localization of WT mGFP-myosin-Va at the tip of the spine ER (Fig. 3) does not reflect simply the myosin's association with the PSD[26], since the myosin and PSD-proteins (PSD-93 and Homer-3a) localize to different albeit closely-opposed sites (Supplementary Information, Fig. S8, Movie 11). An association of myosin-Va with the spine ER is further supported by previous immuno-electron microscopy data showing endogenous myosin-Va on tubulovesicular ER in PN spines[20]. Finally, using three-color imaging of live d^{l20J}/d^{l20J} PNs expressing mGFP-myosin-Va, mRFP-ER, and the cell volume marker mCerulean, we find that the myosin co-localizes with the leading tip of the ER tubule as the tubule moves into a preexisting spine-like protrusion (Fig. 4; Supplementary Movie 12).

So far, our findings are completely consistent with Mechanism 3 (Fig. 1g). A prediction from this model is that attenuation of the myosin's ability to move along actin should lead to a reduction in the robustness of ER targeting and in the speed of ER tubule movement towards the tip of spines. To perform this direct test of myosin-Va-dependent ER motility, we analyzed WT PNs and d^{l20J}/d^{l20J} PNs expressing WT myosin-Va or mutant versions of the myosin that display both reduced velocities and run lengths *in vitro*[29–31]. These mutants were: (i) myosin-Va with a switch 1 mutation that slows the myosin's ATPase activity (myosin-Va^{S217A})[27], and (ii) two versions of myosin-Va with reduced lever arm length (myosin-Va^{4IQ} and myosin-Va^{2IQ}, which contain four or two of the myosin's six IQ motifs, respectively). Reduction of myosin-Va's lever arm length leads to proportional changes in the myosin's step-size *in vitro*[28, 29], and similar lever arm mutations in Myo2p reduce proportionally the velocities of secretory vesicles, a Myo2p cargo in yeast[8].

We initially determined if ER localization to spines is restored in d^{l20J}/d^{l20J} PNs by these mutant myosins at 15 DIV (Fig. 5a). Analysis of d^{l20J}/d^{l20J} PNs expressing GFP-tagged versions of these mutant myosins shows that whereas myosin-Va^{4IQ} rescues ER targeting to the same extent as WT myosin-Va, significantly fewer spines contain ER in the case of both myosin-Va^{2IQ} and myosin-Va^{S217A} (Fig. 5a; Supplementary Movie 10). Similarly, the dendrite morphology defect of d^{l20J}/d^{l20J} PNs is reversed by the expression of WT myosin-Va and myosin-Va^{4IQ}, and partially reversed by the expression of myosin-Va^{2IQ} and myosin-Va^{S217A} (Supplementary Information, Fig. S6).

Strikingly, at 10 DIV, the maximum velocity of ER movement into spines is significantly slower in PNs expressing myosin-Va^{2IQ} or myosin-Va^{S217A} compared to WT PNs and d^{l20J}/d^{l20J} PNs rescued with either WT myosin-Va or myosin-Va^{4IQ} (Fig. 5b, Supplementary Information, Fig. S9). Notably, myosin-Va^{2IQ} and myosin-Va^{S217A}, like WT myosin-Va, are present at the tips of spine ER tubules when expressed as GFP fusions in d^{l20J}/d^{l20J} PNs (Supplementary Information, Fig. S10). We conclude, therefore, that myosin-Va drives the movement of the ER towards the spine tip.

We have shown here that myosin-Va is a point-to-point organelle transporter that translocates ER into PN spines, and that it drives the vast majority of ER insertional movements (although microtubules may make a minor contribution). While previous experiments with cell extracts suggested that myosin-V might mediate ER motility[30, 31], our

results demonstrate for the first time that an actin-based motor in fact moves ER within animal cells. This function, which may be evolutionarily ancient[32, 33], complements the recent demonstration that myosin-Vb moves recycling endosomes into the dendritic spines of hippocampal neurons[34]. Given that microtubules play a crucial role in ER distribution and movement in neuronal dendrites[13, 35], our results also establish a clear example of the dual-filament model of organelle transport[36]. These findings, together with our confirmation at the single spine level that the mGluR-dependent Ca^{2+} transient is abolished in *dilute-lethal* PN spines, establish that myosin-Va-driven ER motility is crucial for at least one physiological function of the ER (local Ca^{2+} release required for PF-PN LTD). Moreover, we suggest that the myosin-Va-mediated translocation of Itpr1-laden ER may be of general importance for Itpr1-mediated calcium signaling in the nervous system (see e.g.[15, 37]), since the neurological phenotype of *dilute-lethal* mice[10] is strikingly similar to that of *Itpr1* mutant mice[16] and much more severe than that of mice merely lacking PF-PN LTD[17].

Methods

Two-photon laser uncaging of MNI-glutamate and Ca^{2+} imaging in PN spines

Parasagittal slices (250 μm thick) were cut from the cerebellar vermis of d^{v}/d^{l20J} or d^{l20J}/d^{l20J} mice at postnatal day P15 to P17. Dissections were performed in an ice-cold sucrose solution containing the following (in mM): 75 NaCl, 26 $NaHCO_3$, 75 sucrose, 25 glucose, 2.5 KCl, 1.25 NaH_2PO_4, 7 $MgCl_2$, and 0.5 $CaCl_2$. Slices were incubated for 30 min at 32°C in sucrose solution, transferred to saline solution (in mM: 125 NaCl, 26 $NaCO_3$, 1.25 NaH_2PO_4, 2.5 KCl, 1 $MgCl_2$, 2 $CaCl_2$, and 25 glucose), and after 30 min allowed to cool to room temperature. All solutions were bubbled with 95% O_2/5% CO_2. Whole-cell recordings were obtained from PNs using differential interference contrast microscopy. Glass electrodes (4 to 6 MΩ) were filled with (in mM): 130 $KMeSO_4$, 10 HEPES, 5 NaCl, 1 $MgCl_2$, 4 Mg-ATP, 0.4 Na-GTP, 14 Tris-phosphocreatine, pH 7.3, 290 mOsm. Electrodes also contained Alexa-594 (20 μM) to visualize cell morphology, and fluo-4 (150 μM) to measure Ca^{2+} signals. Voltage clamp recordings were made with a Multiclamp 700B amplifier (Molecular Devices) filtered at 3 kHz. All recordings were made from slices bathed in the saline solution containing MNI-glutamate (3.75 mM), picrotoxin (20 μM; to block GABA-A receptors) and tetrodotoxin (0.5 μM; to block voltage-gated sodium channels). In some experiments, the AMPA receptor antagonist DNQX (10 μM) and/or the mGluR1 antagonist CPCCOEt (100 μM) were added. Experiments were performed at room temperature. PNs were loaded through the recording pipette for 10 to 20 min before imaging. Combined two-photon laser scanning microscopy and two-photon laser uncaging was performed with a custom-built microscope[41]. The outputs of two Ti:sapphire lasers (Chameleon, Coherent, Santa Clara, CA) were independently modulated with Pockel's cells (Conoptics). The beams were combined using polarization optics and guided to a single pair of scanning galvanometer (Cambridge Technology). The lasers were tuned to 820 nm and 720 nm for imaging and uncaging, respectively. MNI-glutamate was uncaged with three pulses of 1 msec duration delivered at 100 Hz. Line scans were performed at 500 Hz. Fluorescence signals were collected through the objective (60×, 0.9 NA, Olympus) and an oil condenser (1.4 NA, Olympus) and the signals were summed with a current preamplifier (Stanford Instruments) and digitally sampled at 1.25 MHz (PCI-6110, National Instruments).

Fluorescence emission was separated with a dichroic mirror (565DCXR, Chroma) and green and red fluorescence were isolated with bandpass filters (525/50 and 617/73 nm, respectively). Green and red fluorescence was detected with H7422-50 and R9110 photomultiplier tubes, respectively (Hamamatsu). Scanning and signal collection were controlled by custom software written in MATLAB. Laser power for uncaging was adjusted to produce ~40% bleaching of Alexa-594 fluorescence in the spine head[42] to provide consistent power delivery for uncaging at different spines.

Mice

Timed-pregnant C57BL/6J WT mice were purchased from Charles River Laboratories. C57BL/6J mice heterozygous for the *dilute-lethal* allele d^{l20J} and the *dilute-viral* allele d^{v} (i.e. d^{v}/d^{l20J} mice[7, 10]) were mated to obtain d^{l20J}/d^{l20J}, d^{v}/d^{l20J} and d^{v}/d^{v} progeny. In some cases, the d^{v}/d^{l20J} or d^{v}/d^{v} littermate mice or cultures were used as the normal control. This is valid because (i) the d^{v} allele abolishes *Myo5a* expression in the skin but not in the brain[43], (ii) both d^{v}/d^{l20J} and d^{v}/d^{v} mice do not display the neurological phenotype exhibited by d^{l20J}/d^{l20J} mice[10, 43], and (iii) there is no significant difference in the fraction of spines that contain ER, or in the frequency of ER movements into spines, when d^{v}/d^{l20J} PNs are compared with WT PNs (Fig. 5a, Supplementary Information, Fig. S2). Approved protocols were followed for all animal procedures.

Preparation and transfection of dissociated cerebellar cultures

Dissociated cerebellar cultures were prepared from E17 or E18 mouse embryos as described[44], except that the freshly-dissociated cerebellar cells were transfected with novel *L7* (*Pcp-2*)-based expression plasmids using nucleofection (Amaxa/Lonza) (W.W., Seumas McCroskery, and J.A.H., manuscript in preparation). Embryos were obtained from timed-pregnant WT mice or timed-pregnant d^{v}/d^{l20J} mice (yielding d^{l20J}/d^{l20J}, d^{v}/d^{l20J} and d^{v}/d^{v} littermates) and were treated separately during culture preparation, yielding a single culture per embryo. d^{l20J}/d^{l20J} cultures were used for the analyses of the mutant myosin-Va-null phenotype and for the rescue experiments with full-length myosin-Va cDNA. To distinguish between d^{l20J}/d^{l20J}, d^{v}/d^{l20J} and d^{v}/d^{v} cultures, diagnostic PCR was performed on genomic DNA prepared from embryo brain tissue saved during the dissection procedure, using four primers (3'-CACCATCATCTCATTTCCATCCTGTGTCC-5', 3'-CTCAGGAGGATAATAAATGCACGAGACGC-5', 3'-CTCATCTATACATGGTAATAGCAGGTGGC-5', and 3'-CAGTTAGAGAAGGCTAGAAGTAGCAGAGG-5'). This reaction yields a 334 bp fragment for the d^{l20J} allele, and both a 291 bp fragment and a 251 bp fragment in case of either the d^{v} or the WT allele. For all statistical analyses, the mean values ± SEM are indicated, unless indicated otherwise.

DNA Constructs

The PN-specific expression plasmid pL7, which will be described in detail elsewhere (W.W., Seumas McCroskery, and J.A.H., manuscript in preparation), is a Bluescript SK+-based vector that contains (i) a promotor sequence derived from the *L7* (*Pcp-2*) gene that, within the cerebellum, drives expression specifically in the PNs[18], and (ii) a multiple

cloning site inserted into the *Bam*HI site of the *L7* (*Pcp-2*) fragment. This plasmid leads to the specific and efficient expression of inserted cDNAs within PNs present in heterogenous, dissociated cerebellar cultures. Construction of plasmids pL7-mGFP, pL7-mCherry, pL7-mCerulean, pL7-Homer-3a-mGFP, pL7-PSD93-mGFP and pβ-Actin-fGFP will be described elsewhere (W.W., Seumas McCroskery, and J.A.H., manuscript in preparation). To obtain a plasmid that drives the expression of a luminal ER marker under control of the *L7*(*Pcp-2*) promotor, a cDNA encoding a fusion protein (mRFP-ER) consisting of the prolactin signal sequence, mRFP and the KDEL ER retention signal[19] was inserted into plasmid pL7, creating pL7-mRFP-ER. Similarily, pL7-mRFP-ER-IRES-GFP contains the cDNA encoding mRFP-ER, followed by an internal ribosomal entry side and the EGFP cDNA obtained from pIRES2-EGFP (Clontech). Plasmid pL7- ITPKA-9-52-mGFP was created by inserting the *Nhe*I-*Age*I ITPKA-9-52 fragment from N9-52-GFP[45] into the *Nhe*I-*Age*I sites of pL7-mGFP, generating a ITPKA-9-52-mGFP fusion identical to that in N9-52-GFP. To create a plasmid for the expression of α2-tubulin under L7-promotor control, a fragment containing the human α2-tubulin cDNA was inserted downstream of GFP in pL7-mGFP. Plasmids pL7-mGFP-myosin-Va and pL7-mCherry-Myosin-Va correspond to pL7-mGFP and pL7-mCherry, respectively, which contain (in frame and downstream of mGFP or mCherry) the cDNA encoding the full-length, WT, brain-spliced isoform[43] of mouse myosin-Va. Plasmids pL7-mGFP-myosin-Va-R219A, pL7-mGFP-myosin-Va-G440A, pL7-mGFP-myosin-Va-E442A, and pL7-mGFP-myosin-Va-S217A are derivatives of pL7-mGFP-myosin-Va and encode mutant versions of myosin-Va with the indicated single amino acid changes. To create plasmids pL7-mGFP-myosin-Va-4IQ and pL7-mGFP-myosin-Va-2IQ, an *Eco*RI-*Sph*I DNA fragment that encompasses myosin-Va's IQ domain was swapped with the respective mutant fragments from mouse myosin-Va constructs with 4 or 2 IQ motifs[28]. All constructs were confirmed by DNA sequencing.

Microscopy analyses of cerebellar cultures

Cerebellar cultures were imaged using a laser scanning confocal microscope (LSM 510, Carl Zeiss, Inc.) equipped with a 100× objective (1.4 NA). During observation, live cultures were kept at 37 °C and supplied with humidified air containing 5% CO_2. To determine the relative enrichment of F-actin in spines versus dendritic shafts, single confocal plane images of dendrites from PNs expressing both IPTKA-9-52-mGFP and mCherry were recorded, avoiding signal saturation. The average signal intensity of IPTKA-9-52-mGFP along a line placed (i) along the length of the spine and (ii) within the shaft was determined. To correct for differences in sample thickness in shaft versus spine (the latter often being thinner than the confocal section), the average signal intensity of mCherry was measured from the same locations as the IPTKA-9-52-mGFP signal, and the product of the IPTKA-9-52-mGFP-spine signal and mCherry-shaft signal was divided by the mCherry-spine signal. Division of this corrected ITPKA-9-52-mGFP-spine signal by the ITPKA-9-52-mGFP-shaft signal yielded the fold-enrichment of ITPKA-9-52-mGFP in spines. For nocodazole experiments, 2 μl of 200 μM nocodazole stock dissolved in DMSO (or, for control, 2 μl DMSO) were directly added to the culture medium (2 ml), before cultures were mounted on the microscope, and movies were recorded during a period of 15 – 70 min after nocodazole (or DMSO) addition. For the co-culture experiment (Supplementary Information, Fig. S7), freshly dissociated WT cerebellar cells were nucleofected with pβ-Actin-fGFP and mixed 1:1 with freshly

dissociated d^{l20J}/d^{l20J} cerebellar cells prepared at the same time and nucleofected with pL7-mRFP-ER-IRES-EGFP. The cell mix was plated, cultured and imaged as above.

ER motility analysis

To determine (1) the frequency of ER movements into spines, (2) the frequency of spine ER retractions, and (3) the frequency at which spines are found filled with ER, partially filled with ER, or devoid of ER (Supplementary Information, Fig. S2, S3), dual-color movies depicting ER and cell volume were acquired from PNs expressing the luminal ER marker mRFP-ER and free GFP as a cell volume marker. The movies were recorded at a rate of 1 fps for 90 – 150 seconds. The following parameters were determined for each individual spine in these movies: the total time of presence of the spine throughout the movie; the time it was entirely, partially, or not filled with ER; the number of ER translocations into spines (partially or all the way; > 0.3 um); the number of ER retractions (> 0.3 um). Analysis of these data yielded the relative time spines were entirely, partially, or not filled with ER. Furthermore, the frequency of ER translocations into spines was determined by dividing the number of total ER insertions by the time (minutes) during which spines were found partially or not filled with ER (i.e. not already fully loaded). Similarily, the frequency of spine ER retractions from spines was determined by dividing the number of total ER retractions by the time (minutes) during which spines that were found filled or partially filled with ER (i.e. where ER retraction is possible). The maximum velocity of ER movement directed towards the distal end of spines (“spine tip”) was determined in six steps, as follows. Step 1: acquisition of dual-color movies depicting ER and cell volume. Movies of PNs expressing the luminal ER marker mRFP-ER, the cell volume marker GFP and, if applicable, a GFP-tagged version of myosin-Va, were recorded at a rate of 1 fps for 120 seconds using a laser scanning confocal microscope. Step 2: identification of spines with ER movement towards the spine tip. ER translocation into spines was not seen in every spine imaged and, if ER translocation into spines occurred, it was a relatively brief event that took place over ~5 – 20 seconds (see examples in Fig. 2d and Supplementary Information, Movies 1 and 2). Therefore, we inspected movies by eye for spines into which ER clearly translocated and subjected these particular spines to kymograph analysis. Step 3: kymograph analysis. Using MetaMorph software (MDS Analytical Technologies), kymographs of cell volume and ER were obtained from spines selected in step 2 by placing a line along the protrusion and precisely in the same direction as the translocating ER. Kymograph analysis was terminated if the spine tilted relative to the kymograph line or moved away from it. Examples of kymographs are shown in Supplementary Information, Figure S9. To facilitate the measurement of the ER's instantaneous velocity (i.e. the distance that the ER traveled within the 1 second-long interval between movie frames), the position of the ER's leading edge and the spine tip were manually determined from the kymograph images at each 1 second interval, and this positional data was recorded in spreadsheets. Graphs generated from these positional data (as well as the kymographs themselves) revealed periods of forward ER movement into spines, but also periods of ER retraction and periods where the ER paused (see examples in Supplementary Information, Figure S5). Step 4: identification of periods of persistent ER movement towards the spine tip. We established specific criteria to select forward ER motility periods from the positional data. These criteria served to limit our measurements to those periods where the ER is undergoing a persistent

movement towards the spine tip (the movement that we hypothesized is myosin-Va-driven), and to exclude from our analyses (i) periods where the ER was fully inserted into the spine, and (ii) periods where the ER was undergoing persistent movement away from the spine tip (i.e. periods of retraction). These specific criteria were: (i) the spine ER must make a net forward movement of at least 0.46 μm (i.e. 5 pixels; 1 pixel corresponding to 92 nm) towards the spine tip before or upon reaching the spine tip (i.e. getting as close as 2 pixels, or less, to the volume marker's front), and (ii) the ER must move as defined in (i) without retracting in two or more frames that are either consecutive or spaced by frames without detectable ER movement. In addition, periods of ER motility were further defined to start at the time when the ER was at its lowest (least inserted) position that was closest to the end of the forward motility period. Finally, periods of ER motility ended as soon as the ER reached its outmost (most distal) position for the first time. We note that, according to our criteria, instances where the ER (i) retracts for just a single frame, or (ii) pauses for an unlimited number of consecutive frames (as long as these pauses do not occur at the beginning or end of forward ER motility events), are considered a part of forward ER motility events. The bold portions of the lines in the graphic rendering of the kymographs in Supplementary Information Figure S5 show examples of periods of forward ER motility that were identified based on these criteria. The total numbers of such forward ER motility periods identified and used for further analysis were: 18 for WT; 32 for d^{l20J}/d^{l20J} + MVa-WT; 41 for d^{l20J}/d^{l20J} + MVa-4IQ; 46 for d^{l20J}/d^{l20J} + MVa-2IQ; and 19 for d^{l20J}/d^{l20J} + MVa-S217A. Step 5: measurement of the instantaneous velocities of ER movement. The distance that the ER moved within one second (i.e. its instantaneous velocity) during periods of forward motility, as defined in step 4, was calculated from the positional data in the spreadsheets. As expected, we obtained three classes of instantaneous ER velocities that occurred from one frame to the next (i.e. within one second) for each experimental condition: towards the spine tip (+), away from the spine tip (−), and no movement at all (0). The total numbers of instantaneous ER velocities that were measured and used for further analysis were: 122 for WT; 282 for d^{l20J}/d^{l20J} + MVa-WT; 355 for d^{l20J}/d^{l20J} + MVa-4IQ; 466 for d^{l20J}/d^{l20J} + MVa-2IQ; and 193 for d^{l20J}/d^{l20J} + MVa-S217A. Importantly, for each experimental condition, a similar percentage of the measured instantaneous velocities was (+), i.e. directed towards the spine tip (see below). Step 6: calculation of the maximum velocity of ER movement directed towards the spine tip from the (+) instantaneous velocities of ER movement. Because we wanted to test if myosin-Va specifically drives the forward movement of ER into spines, only those instantaneous ER velocities collected from the motility periods that were directed towards the spine tip (i.e. the instantaneous (+) velocities) were considered for calculating the maximum velocity of ER movement towards the spine tip. The total numbers of instantaneous (+) velocities were: 91 for WT (74.6% of the total instantaneous ER velocities); 207 for d^{l20J}/d^{l20J} + MVa-WT (73.4% of the total instantaneous ER velocities); 264 for d^{l20J}/d^{l20J} + MVa-4IQ (74.4% of the total instantaneous ER velocities); 350 for d^{l20J}/d^{l20J} + MVa-2IQ (75.1% of the total instantaneous ER velocities); and 133 for d^{l20J}/d^{l20J} + MVa-S217A (68.9% of the total instantaneous ER velocities). The maximum velocities shown in the graph in Fig. 5b were obtained by averaging the fastest 10% of these instantaneous (+) velocities.

Supplementary Material

Refer to Web version on PubMed Central for supplementary material.

Acknowledgements

We thank Roland Bock and David J. Linden (Johns Hopkins University, Baltimore) for teaching us cerebellar culture preparation, John Oberdick (The Ohio State University, Columbus), Erik L. Snapp and Jennifer Lippincott-Schwartz (NICHD, NIH, Bethesda), Howard D. White (Eastern Virginia Medical School, Norfolk), James R. Sellers, Jose A. Martina and Seumas McCroskery (NHLBI, NIH, Bethesda), Michael J. Schell (Uniformed Services University, Bethesda) and David S. Bredt (University of California, San Francisco) for DNA constructs, Richard E. Cheney (University of North Carolina, Chapel Hill) for advice, and Xufeng Wu (NHLBI, NIH, Bethesda) for microscopy support.

References

1. Miyata M, et al. Local calcium release in dendritic spines required for long-term synaptic depression. Neuron. 2000; 28:233–244. [PubMed: 11086997]
2. Takagishi Y, et al. The *dilute-lethal* (d^l) gene attacks a Ca^{2+} store in the dendritic spine of Purkinje cells in mice. Neurosci. Lett. 1996; 215:169–172. [PubMed: 8899740]
3. Sellers, JR.; Weisman, LS.; Myosin, V. Myosins: A Superfamily of Molecular Motors. Springer; Netherlands: 2008.
4. Woolner S, Bement WM. Unconventional myosins acting unconventionally. Trends Cell Biol. 2009; 19:245–252. [PubMed: 19406643]
5. Desnos C, et al. Myosin Va mediates docking of secretory granules at the plasma membrane. J. Neurosci. 2007; 27:10636–10645. [PubMed: 17898234]
6. Provance DW Jr. et al. Myosin-Vb functions as a dynamic tether for peripheral endocytic compartments during transferrin trafficking. BMC Cell Biol. 2008; 9:44. [PubMed: 18687135]
7. Wu X, Bowers B, Rao K, Wei Q, Hammer JA 3rd. Visualization of melanosome dynamics within wild-type and *dilute* melanocytes suggests a paradigm for myosin V function *in vivo*. J. Cell Biol. 1998; 143:1899–1918. [PubMed: 9864363]
8. Schott DH, Collins RN, Bretscher A. Secretory vesicle transport velocity in living cells depends on the myosin-V lever arm length. J. Cell Biol. 2002; 156:35–39. [PubMed: 11781333]
9. Jung G, Titus MA, Hammer JA 3rd. The *Dictyostelium* type V myosin MyoJ is responsible for the cortical association and motility of contractile vacuole membranes. J. Cell Biol. 2009; 186:555–570. [PubMed: 19687255]
10. Strobel MC, Seperack PK, Copeland NG, Jenkins NA. Molecular analysis of two mouse *dilute* locus deletion mutations: spontaneous *dilute lethal*^{20J} and radiation-induced *dilute prenatal lethal Aa2* alleles. Mol. Cell. Biol. 1990; 10:501–509. [PubMed: 2300051]
11. Tilelli CQ, Martins AR, Larson RE, Garcia-Cairasco N. Immunohistochemical localization of myosin Va in the adult rat brain. Neuroscience. 2003; 121:573–586. [PubMed: 14568019]
12. Bourne JN, Harris KM. Balancing structure and function at hippocampal dendritic spines. Annu. Rev. Neurosci. 2008; 31:47–67. [PubMed: 18284372]
13. English AR, Zurek N, Voeltz GK. Peripheral ER structure and function. Curr. Opin. Cell Biol. 2009; 21:596–602. [PubMed: 19447593]
14. Hartmann J, Konnerth A. Mechanisms of metabotropic glutamate receptor-mediated synaptic signaling in cerebellar Purkinje cells. Acta Physiol. (Oxf.). 2008
15. Holbro N, Grunditz A, Oertner TG. Differential distribution of endoplasmic reticulum controls metabotropic signaling and plasticity at hippocampal synapses. Proc. Natl. Acad. Sci. U. S. A. 2009; 106:15055–15060. [PubMed: 19706463]
16. Matsumoto M, Nagata E. Type 1 inositol 1,4,5-trisphosphate receptor knockout mice: their phenotypes and their meaning in neuroscience and clinical practice. J. Mol. Med. 1999; 77:406–411. [PubMed: 10426189]

17. De Zeeuw CI, et al. Expression of a protein kinase C inhibitor in Purkinje cells blocks cerebellar LTD and adaptation of the vestibulo-ocular reflex. Neuron. 1998; 20:495–508. [PubMed: 9539124]
18. Serinagaoglu Y, et al. A promoter element with enhancer properties, and the orphan nuclear receptor RORalpha, are required for Purkinje cell-specific expression of a $G_{i/o}$ modulator. Mol. Cell. Neurosci. 2007; 34:324–342. [PubMed: 17215137]
19. Altan-Bonnet N, et al. Golgi inheritance in mammalian cells is mediated through endoplasmic reticulum export activities. Mol. Biol. Cell. 2006; 17:990–1005. [PubMed: 16314396]
20. Petralia RS, et al. Glutamate receptor targeting in the postsynaptic spine involves mechanisms that are independent of myosin Va. Eur. J. Neurosci. 2001; 13:1722–1732. [PubMed: 11359524]
21. Hoogenraad CC, Bradke F. Control of neuronal polarity and plasticity - a renaissance for microtubules? Trends Cell Biol. 2009; 19:669–676. [PubMed: 19801190]
22. Linden DJ, Ahn S. Activation of presynaptic cAMP-dependent protein kinase is required for induction of cerebellar long-term potentiation. J. Neurosci. 1999; 19:10221–10227. [PubMed: 10575019]
23. Hisatsune C, et al. Inositol 1,4,5-trisphosphate receptor type 1 in granule cells, not in Purkinje cells, regulates the dendritic morphology of Purkinje cells through brain-derived neurotrophic factor production. J. Neurosci. 2006; 26:10916–10924. [PubMed: 17050730]
24. Yengo CM, De la Cruz EM, Safer D, Ostap EM, Sweeney HL. Kinetic characterization of the weak binding states of myosin V. Biochemistry. 2002; 41:8508–8517. [PubMed: 12081502]
25. Shimada T, Sasaki N, Ohkura R, Sutoh K. Alanine scanning mutagenesis of the switch I region in the ATPase site of *Dictyostelium discoideum* myosin II. Biochemistry. 1997; 36:14037–14043. [PubMed: 9369475]
26. Walikonis RS, et al. Identification of proteins in the postsynaptic density fraction by mass spectrometry. J. Neurosci. 2000; 20:4069–4080. [PubMed: 10818142]
27. Forgacs E, et al. Switch 1 mutation S217A converts myosin V into a low duty ratio motor. J. Biol. Chem. 2009; 284:2138–2149. [PubMed: 19008235]
28. Sakamoto T, Yildez A, Selvin PR, Sellers JR. Step-size is determined by neck length in myosin V. Biochemistry. 2005; 44:16203–16210. [PubMed: 16331980]
29. Purcell TJ, Morris C, Spudich JA, Sweeney HL. Role of the lever arm in the processive stepping of myosin V. Proc. Natl. Acad. Sci. U. S. A. 2002; 99:14159–14164. [PubMed: 12386339]
30. Wollert T, Weiss DG, Gerdes HH, Kuznetsov SA. Activation of myosin V-based motility and F-actin-dependent network formation of endoplasmic reticulum during mitosis. J. Cell Biol. 2002; 159:571–577. [PubMed: 12438410]
31. Tabb JS, Molyneaux BJ, Cohen DL, Kuznetsov SA, Langford GM. Transport of ER vesicles on actin filaments in neurons by myosin V. J. Cell Sci. 1998; 111:3221–3234. [PubMed: 9763516]
32. Yokota E, et al. An isoform of myosin XI is responsible for the translocation of endoplasmic reticulum in tobacco cultured BY-2 cells. J. Exp. Bot. 2009; 60:197–212. [PubMed: 19039101]
33. Estrada P, et al. Myo4p and She3p are required for cortical ER inheritance in *Saccharomyces cerevisiae*. J. Cell Biol. 2003; 163:1255–1266. [PubMed: 14691136]
34. Wang Z, et al. Myosin Vb mobilizes recycling endosomes and AMPA receptors for postsynaptic plasticity. Cell. 2008; 135:535–548. [PubMed: 18984164]
35. Bannai H, Inoue T, Nakayama T, Hattori M, Mikoshiba K. Kinesin dependent, rapid, bi-directional transport of ER sub-compartment in dendrites of hippocampal neurons. J. Cell Sci. 2004; 117:163–175. [PubMed: 14676272]
36. Langford GM. Actin- and microtubule-dependent organelle motors: interrelationships between the two motility systems. Curr. Opin. Cell Biol. 1995; 7:82–88. [PubMed: 7755993]
37. Toresson H, Grant SG. Dynamic distribution of endoplasmic reticulum in hippocampal neuron dendritic spines. Eur. J. Neurosci. 2005; 22:1793–1798. [PubMed: 16197520]
38. Bittins CM, Eichler TW, Gerdes HH. Expression of the dominant-negative tail of myosin Va enhances exocytosis of large dense core vesicles in neurons. Cell. Mol. Neurobiol. 2009; 29:597–608. [PubMed: 19214741]

39. Watanabe M, et al. Myosin-Va regulates exocytosis through the submicromolar Ca^{2+}-dependent binding of syntaxin-1A. Mol. Biol. Cell. 2005; 16:4519–4530. [PubMed: 16030255]

40. Shiraishi-Yamaguchi Y, Furuichi T. The Homer family proteins. Genome Biol. 2007; 8:206. [PubMed: 17316461]

41. Carter AG, Sabatini BL. State-dependent calcium signaling in dendritic spines of striatal medium spiny neurons. Neuron. 2004; 44:483–493. [PubMed: 15504328]

42. Bloodgood BL, Sabatini BL. Nonlinear regulation of unitary synaptic signals by $CaV_{2.3}$ voltage-sensitive calcium channels located in dendritic spines. Neuron. 2007; 53:249–260. [PubMed: 17224406]

43. Seperack PK, Mercer JA, Strobel MC, Copeland NG, Jenkins NA. Retroviral sequences located within an intron of the *dilute* gene alter *dilute* expression in a tissue-specific manner. EMBO J. 1995; 14:2326–2332. [PubMed: 7774591]

44. Tabata T, et al. A reliable method for culture of dissociated mouse cerebellar cells enriched for Purkinje neurons. J. Neurosci. Methods. 2000; 104:45–53. [PubMed: 11163410]

45. Johnson HW, Schell MJ. Neuronal IP_3 3-kinase is an F-actin bundling protein: role in dendritic targeting and regulation of spine morphology. Mol. Biol. Cell. 2009; 20:5166–5180. [PubMed: 19846664]

46. Harris KM, Stevens JK. Dendritic spines of rat cerebellar Purkinje cells: serial electron microscopy with reference to their biophysical characteristics. J. Neurosci. 1988; 8:4455–4469. [PubMed: 3199186]

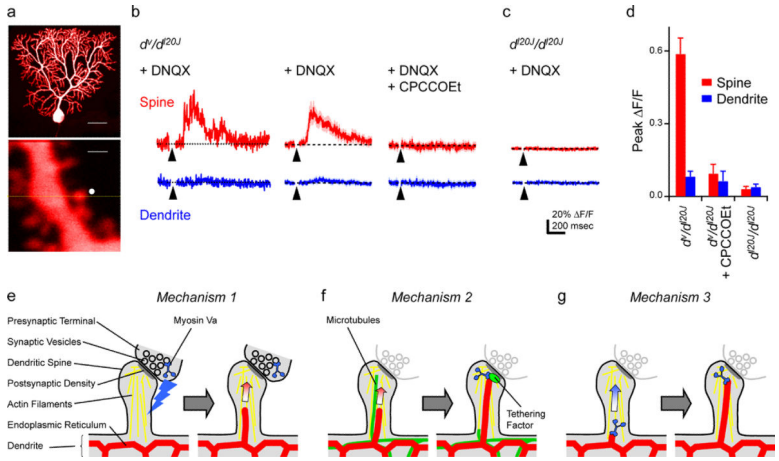

Figure 1. Absence of the delayed mGluR1-dependent Ca^{2+} transient in d^{l20J}/d^{l20J} PN spines and hypothetical models for how myosin-Va might function to localize the ER Ca^{2+} store to spines

(**a**) Images of a PN (upper panel; size bar, 30 μm) and a PN dendrite and spine (lower panel; size bar, 1 μm). PNs in cerebellar slices were voltage clamped at −70 mV, loaded with Ca^{2+} indicator Fluo-4 (150 μM) and red fluorophore Alexa-594 (20 μM) through the recording electrode, and imaged by two-photon laser scanning microscopy. In the lower panel, the white circle indicates the location of two-photon laser uncaging of MNI-glutamate (3.75 mM), and the yellow line indicates the line scan region. (**b**) Ca^{2+} transients in d^{v}/d^{l20J} PN spines (red traces) and adjacent dendritic shafts (blue traces) evoked by glutamate uncaging at the spine head at the time indicated (arrowhead), in the presence of DNQX (10 μM; left and middle panels), or in the additional presence of mGluR1 antagonist CPCCOEt (100 μM; right panel). Left panel: traces from a single trial from the spine depicted in **a**. Middle and right panels: group data for 23 spines (4 PNs) and 20 spines (3 PNs), respectively. The solid traces indicate the mean and the shaded areas indicate SEM. (**c**) CPCCOEt-sensitive Ca^{2+} transients are not observed in d^{l20J}/d^{l20J} PN spines following glutamate uncaging in the presence of DNQX (compare with **b**, middle panel). The mean Ca^{2+} traces (± SEM) from group data for 45 spines (4 PNs) are shown. (**d**) Shown are the average Ca^{2+} transient peak magnitudes (ΔF/F mean ± SEM) in spines (red bars) and dendrites (blue bars) of d^{v}/d^{l20J} and d^{l20J}/d^{l20J} PNs. (**e**) Mechanism 1 (non-cell autonomous model): Myosin-Va present within another cerebellar cell type such as a granule neuron facilitates the release of a diffusible factor that confers upon the PN the ability to target ER to its spines. Relevant to this model, myosin-Va is a synaptic vesicle-associated protein that plays a role in regulating exocytosis[5, 38, 39], and is widely expressed throughout the brain, including within granule neurons[11]. (**f**) Mechanism 2 (tethering model): Myosin-Va delivers a tethering factor to the spine tip that links the ER to the spine tip following the myosin-Va-independent transport of ER into the spine. In this case, ER motility might be microtubule-based, as microtubules transiently enter the spines of hippocampal neurons[21], and microtubule plus end-directed motors are known to transport ER[13, 35]. Alternatively, a direct interaction between the microtubule plus end tracking proteins EB1/3 and the integral ER membrane protein STIM1 might drive the movement of ER tubules into spines[13]. With regard to myosin-Va-dependent tethering, candidates for tethering proteins that might link the ER to the spine tip, such as Homer, are present in PN spines[40]. Alternatively, the myosin itself could be an integral

component of the tethering mechanism[4–7]. (**g**) Mechanism 3 (transport model): Myosin-Va associates with the ER and transports it along actin filaments into spines. In the simplest case, the ER is then maintained at the spine tip via the continued effort of myosin-Va to carry it to the barbed end of actin filaments. We note, however, that the myosin-Va-mediated transport of ER into spines envisioned by Mechanism 3 could be followed by the maintenance of the ER within spines via a secondary tethering mechanism that is by definition myosin-Va-dependent either because it occurs only after the myosin has delivered the ER to the vicinity of the spine tip, or because once there, the myosin is an essential component of the tethering mechanism.

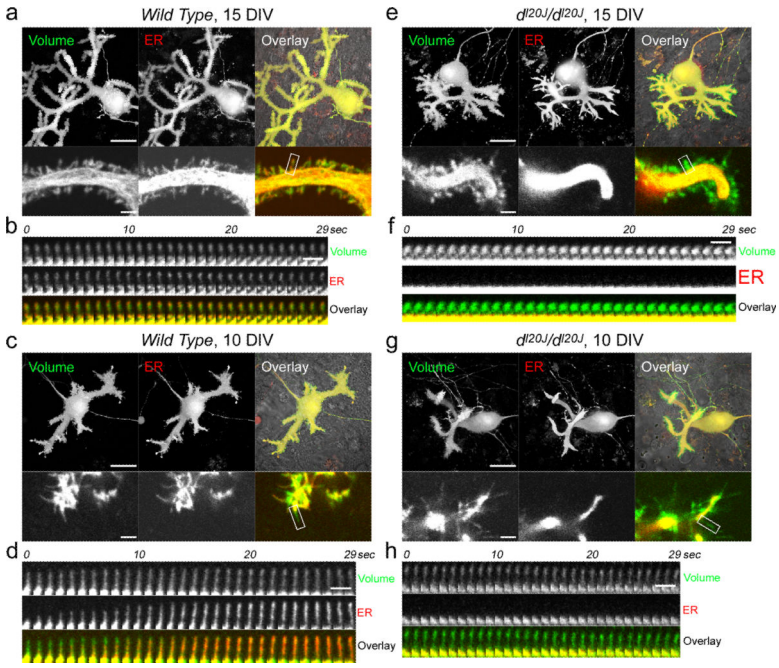

Figure 2. The translocation of ER into spines is disrupted in d^{l20J}/d^{l20J} PNs

Shown are cultured, live PNs from WT mice at 15 DIV (**a, b**) and at 10 DIV (**c, d**), and from d^{l20J}/d^{l20J} mice at 15 DIV (**e, f**) and at 10 DIV (**g, h**). Cultures were transfected with pL7-mRFP-ER-IRES-EGFP to visualize cell volume (*Volume*) and ER (*ER*). Superimpositions are also shown (*Overlay*). The upper panels in **a**, **c**, **e**, and **g** are images reconstructed from confocal Z-stacks (size bar, 20 μm), whereas the lower panels show magnified images of a single confocal plane of PN dendrites (size bar, 2 μm). The latter images were taken from a time series (Supplementary Movies 1, 3). **b**, **d**, **f**, and **h** show montages of 30 consecutive frames of a time series and depict the spines in the white boxes in **a**, **c**, **e**, and **g**, respectively, at higher magnification (size bar, 2 μm; see also Supplementary Movies 2, 4).

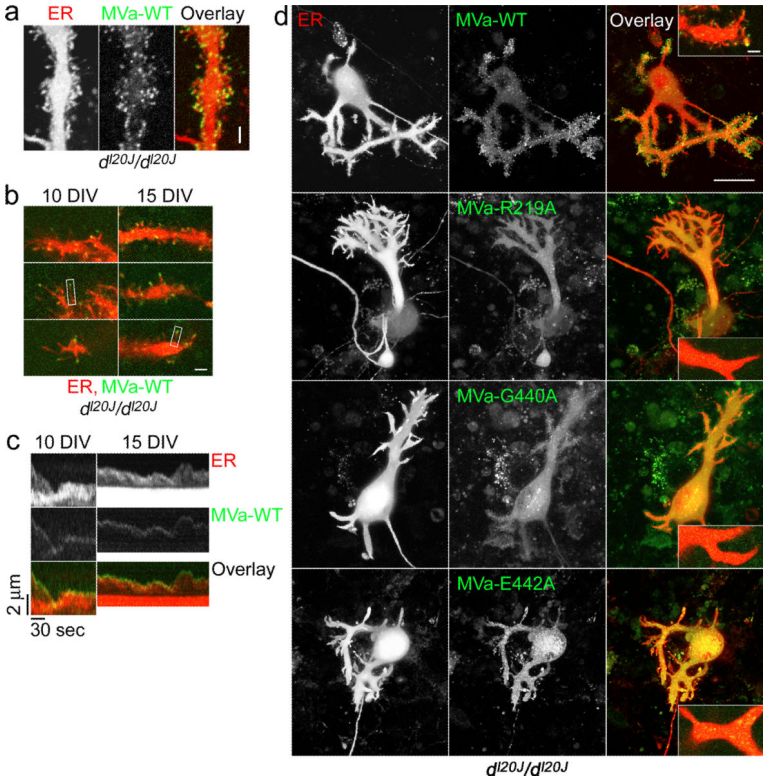

Figure 3. mGFP-myosin-Va expressed in d^{l20J}/d^{l20J} PNs rescues ER targeting and accumulates at the tip of the spine ER

(**a–c**) Shown are live d^{l20J}/d^{l20J} PNs transfected with pL7-mRFP-ER and pL7-mGFP-myosin-Va to visualize the ER (*ER*) and the myosin (*MVa-WT*), respectively. Size bars, 2 µm. **a** shows a maximum projection of a confocal Z-stack of a section of a PN dendrite at 15 DIV (see Supplementary Movie 6 for the corresponding three-dimensional reconstruction). **b** shows images corresponding to single confocal planes of PN dendrites at 10 DIV or 15 DIV. Three examples are shown for each time point. The images were taken from time series (Supplementary Movies 7, 8). The white boxes indicate the spines from which the kymograph images shown in **c** were obtained. The kymographs in **c** show that the dot of mGFP-myosin-Va fluorescence remains present at the distal tip of the ER tubule as the tubule extends or shortens over time. The *x*-axis corresponds to time, the *y*-axis corresponds to size. (**d**) Shown are live d^{l20J}/d^{l20J} PNs transfected with pL7-mRFP-ER to visualize the ER (*ER*) and either pL7-mGFP-myosin-Va (*MVa-WT*), pL7-mGFP-myosin-Va-R219A (*MVa-R219A*), pL7-mGFP-myosin-Va-G440A (*MVa-G440A*) or pL7-mGFP-myosin-Va-E442A (*MVa-E442A*). Images were reconstructed from confocal Z-stacks and depict cells at 13 DIV. Superimposition of images is also shown (*Overlay*). Size bar, 20 µm. Each insert in the overlay images shows a single confocal plane image of a dendrite from a PN transfected with the respective plasmids and depicts ER (red) and myosin (green). Images were taken from a time series (Supplementary Movie 9). Size bar, 2 µm.

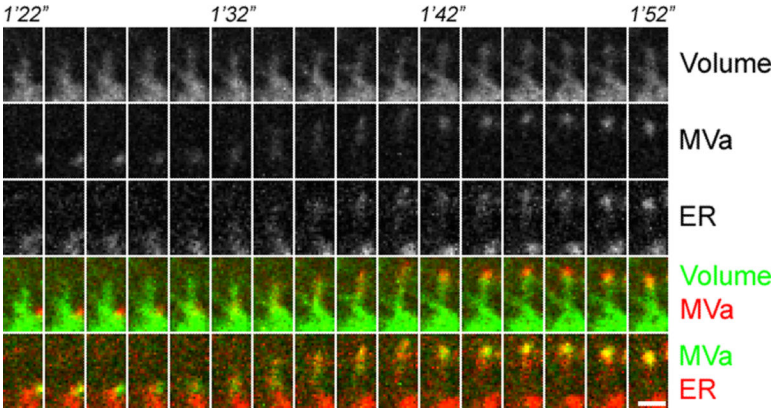

Figure 4. Myosin-Va is present at the leading tip of the ER tubule as the organelle translocates into a spine

Shown is a live d^{l20J}/d^{l20J} PN transfected with pL7-mCerulean, pL7-mGFP-myosin-Va and pL7-mRFP-ER to visualize cell volume (*Volume*), myosin-Va (*MVa*) and ER (*ER*), respectively. Superimpositions of volume and myosin-Va (*Volume MVa*) and myosin-Va and ER (*MVa ER*) are also shown. Images show a single confocal plane and were taken from a time series recorded at a rate of 0.5 frames per second (fps) at DIV 8 (see also Supplementary Movie 12). Size bar, 1 μm.

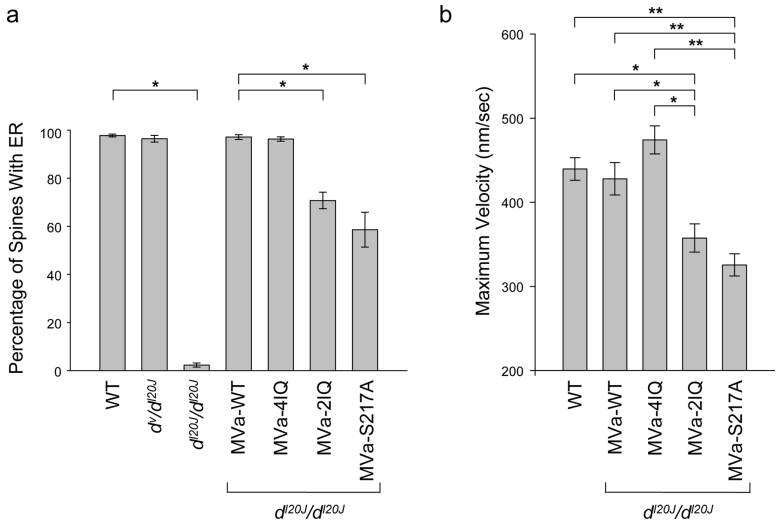

Figure 5. Decreasing the step size or ATPase activity of myosin-Va reduces the efficiency of ER targeting to PN spines and the maximum velocity of ER movement into spines

WT, d^{v}/d^{l20J}, and d^{l20J}/d^{l20J} PNs expressing mRFP-ER to visualize ER and free GFP to visualize cell volume, as well as d^{l20J}/d^{l20J} PNs expressing GFP-tagged versions of WT myosin-Va (*MVa-WT*), myosin-Va^{4IQ} (*MVa-4IQ*), myosin-Va^{2IQ} (*MVa-2IQ*) or myosin-Va^{S217A} (*MVa-S217A*) in addition to mRFP-ER and free GFP were observed using confocal live microscopy. (**a**) The graph shows the fraction of spines (mean ± SEM) that contain ER, as determined from images of PN dendrites recorded at DIV 15. The numbers of analyzed PNs were 15 (WT), 18 (d^{v}/d^{l20J}), 16 (d^{l20J}/d^{l20J}), 21 (*MVa-WT*), 6 (*MVa-4IQ*), 22 (*MVa-2IQ*), and 17 (*MVa-S217A*). On average, 23.5 spines/PN were analyzed. *p< 0.0001; p-values calculated using the Student t-test. See Supplementary Movie 10 for examples. (**b**) Instantaneous velocities of ER movements were measured at DIV 10, as described in Methods and Supplementary Information, Fig. S9. The graph shows the maximum velocity calculated by averaging the fastest 10% of instantaneous movements directed towards the spine tip (error bars indicate SEM). The total numbers of instantaneous velocities determined were 91 (WT), 207 (d^{l20J}/d^{l20J}), 264 (MVa-4IQ), 350 (MVa-2IQ), and 133 (MVa-S217A). *p< 0.05; **p<0.0005, p-values calculated using the Student t-test. Given the motility and processivity defects observed for myosin-Va^{2IQ} and myosin-Va^{S217A} *in vitro*[27–29], it is notable how well these mutants function to move ER in PNs. This could be indicative of ER transport being mediated by an ensemble of myosin-Va molecules.